ACS Energy LETTERS

Cite This: ACS Energy Lett. 2019, 4, 1650−1657

http://pubs.acs.org/journal/aelccp

In Situ Formation of a Stable Interface in Solid-State Batteries

Lilu Liu,[†,§,#] Xingguo Qi,[†,#] Shijun Yin,[†,‡] Qiangqiang Zhang,[†,‡] Xiaozhi Liu,[†] Liumin Suo,[*,†] Hong Li,[†,‡,§,∥] Liquan Chen,[†,‡,§,∥] and Yong-Sheng Hu[*,†,‡,∥]

[†] Key Laboratory for Renewable Energy, Beijing Key Laboratory for New Energy Materials and Devices, Beijing National Laboratory for Condensed Matter Physics, Institute of Physics, Chinese Academy of Sciences, Beijing 100190, China

[‡] Center of Materials Science and Optoelectronics Engineering, University of Chinese Academy of Sciences, Beijing 100049, China

[§] Tianmu Lake Institute of Advanced Energy Storage Technologies Co. Ltd., Liyang 213300, China

[∥] Yangtze River Delta Physics Research Center Co. Ltd., Liyang 213300, China

Supporting Information

ABSTRACT: **Solid polymer electrolytes (SPEs) are considered as promising candidates for solid-state batteries. SPEs with a conventional solution casting technique have serious side reactions during charging because of the residual solvent. Here we report a creative method that can self-remove it via spontaneous reactions. The core idea is to consume the residual solvent and form stable products by choosing proper salt, solvent, and additives. Inspired by the hydrolysis of sodium bis(fluorosulfonyl)imide (NaFSI), during which the proton carrier changes from H_2O to HF and HF further reacts with metal oxide to form a stable hydrate, like $AlF_3 \cdot 6H_2O$, NaFSI, H_2O, and Al_2O_3/SiO_2 nanoparticles are thus employed to prepare poly(ethylene oxide) (PEO)-based SPEs. Solid-state sodium batteries with PEO/NaFSI-Al_2O_3-AQ electrolytes exhibit good reversibility with $Na_3V_2(PO_4)_3$ as the active materials, high rate performance, long-term cycling stability (92.8% after 2000 cycle), and high Coulombic efficiency. Furthermore, environmentally friendly and low-cost preparation of PEO-based SPEs is realized with this aqueous technique.**

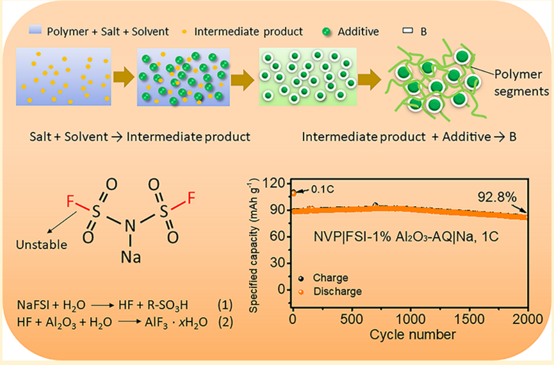

Na ion batteries (NIBs) are considered as promising candidates for grid energy storage systems due to the abundance and low cost of sodium resources.[1−3] Traditional NIBs with organic liquid electrolytes may encounter safety issues because of the flammability of organic solvents.[4−9] Therefore, we have shifted our research interest to all-solid-state batteries, which are intrinsically safer owing to their nonflammable nature.

As the key component in solid-state batteries (SSBs), solid-state electrolytes have attracted worldwide attention. Several types of solid electrolytes for SSBs have been proposed, including β''-Al_2O_3,[10] Na^+ super ionic conductor (NASICON),[11] sulfides,[12,13] and polymers.[14] Among these candidates, ceramic electrolytes (β''-Al_2O_3 and NASICON-type solid electrolytes) usually exhibit high ionic conductivity and good compatibility with cathode materials, though their hardness is also relatively high, which leads to poor point—point contact between the electrode and electrolyte and difficulties in their processing, finally resulting in high contact resistance and manufacture cost.[8,15−17] On the contrary, with their soft nature and a relatively low synthesized temperature, sulfides have the advantages of cost-effectiveness and high ionic conductivity.[18−20] However, their incompatibility with conventional oxide cathode materials and their instability in moist air limit their applications.[21,22] Solid polymer electrolytes (SPEs), in general, possess moderate ionic conductivities, favorable mechanical properties, good flexibilities, and easy processing characteristics and are thus considered one of the most promising candidates for application in SSBs.[23]

A SPE for NIBs usually consists of Na salts (such as sodium bis(fluorosulfonyl)imide (NaFSI), sodium perchlorate ($NaClO_4$), and sodium bis(trifluoromethanesulfonyl)imide (NaTFSI)) and a polymer matrix (including poly(ethylene oxide) (PEO), polyacrylonitrile (PAN), polypropylene carbonate (PPC), and poly(methyl methacrylate) (PMMA)).[4,24] Among them, PEO is absolutely an ideal polymer host by virtue of its good viscoelasticity, high solvation power, complexation, and ion dissociation capability.[25] Considering scaling up the manufacturing process in the future, a feasible solution-casting technique could be adopted by which the

Received: April 21, 2019
Accepted: June 18, 2019
Published: June 18, 2019

DOI: 10.1021/acsenergylett.9b00857
ACS Energy Lett. 2019, 4, 1650−1657

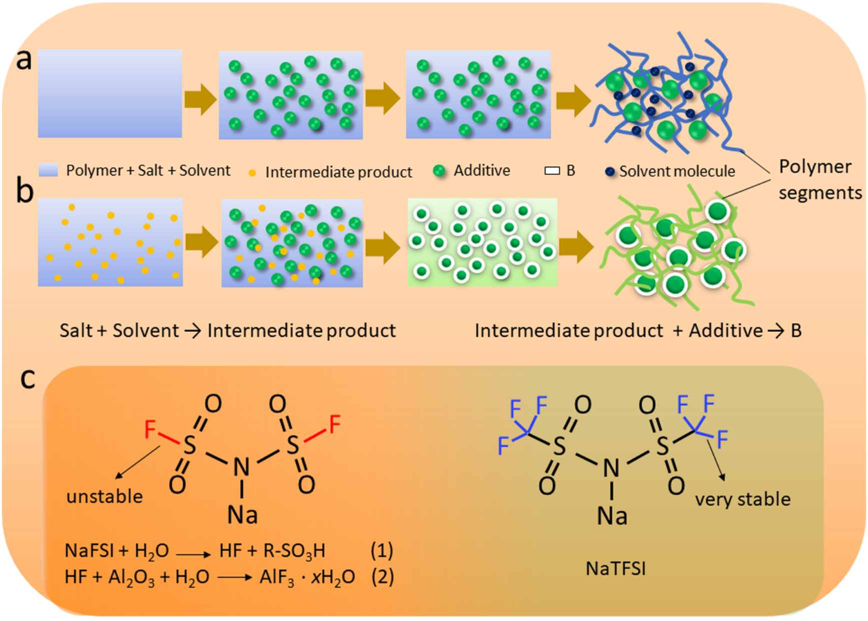

Figure 1. Schematic diagrams of SPE preparation and the chemical structure of Na salt. (a) Traditional process of SPE preparation. (b) Designe process of SPE preparation: the salt reacts with the solvent, and the intermediate product is turned into a stable product B by the additive. (c) Chemical structure of the NaFSI (left) and the NaTFSI (right).

initial electrolyte membrane is dried in a vacuum oven to lower the residual solvent.[26−28] However, due to the strong solvent absorption ability of electrolyte salts, the residual liquid-absorbed solvent in the SPEs is indeed difficult to thoroughly remove only by the simple vacuum process, resulting in low Coulombic efficiencies in the following charge−discharge process due to inevitably irreversible side reactions and decomposition. Compared with the physical vacuum method, the chemical method can effectively remove the solvent on a molecular level and be more helpful for removal of trace solvents remaining in SPEs.

Herein, we design a novel synthesis route for PEO-based SPEs with the function of removing the residual free solvent, which can be consumed spontaneously by the reaction with a salt, whose product can be fixed with an additive through an acid−alkaline neutralization reaction. The process can be depicted as follows:

$$\text{salt} + \text{solvent} + \text{A} \rightarrow \text{B}$$

A is a kind of oxide acting as a proton acceptor, which can react with an acid to form a stable product, B. On the basis of this philosophy, an aqueous PEO/NaFSI-Al_2O_3 SPE (abbreviated as FSI-Al_2O_3-AQ) was selected, where the salt, the solvent, A, and B are NaFSI, distilled water (H_2O), Al_2O_3, and $AlF_3 \cdot xH_2O$, respectively. Al_2O_3 has already been reported to be adopted as an additive in PEO polymer, however, without the research purpose in residue solvent consumption.[29]

Solid-state sodium batteries with this SPE exhibit wonderful electrochemical performance. When carbon-coated $Na_3V_2(PO_4)_3$ (NVP) and Na metal were adopted as the cathode and anode, respectively, the initial reversible specific capacity of the cell was 110 mAh g^{-1}, and the capacity retention was up to 92.8% after 2000 cycles at a rate of 1C, with high Coulombic efficiency (∼100%). To verify the peculiarity of the designed FSI-Al_2O_3-AQ SPE, X-ray photoelectron spectroscopy (XPS), Fourier transform infrared spectroscopy (FTIR), and transmission electron microscopy (TEM) were carried out. Furthermore, PEO/NaFSI-Al_2O_3 electrolyte with acetonitrile as the solvent (abbreviated as FSI-Al_2O_3-AN) and PEO/NaTFSI-Al_2O_3 electrolyte with water as the solvent (abbreviated as TFSI-Al_2O_3-AQ) were also prepared for comparison.

Figure 1a,b shows the schematic diagrams of our strategy. If the selection criterion for the salt is based only on the dissolubility, both NaFSI and NaTFSI with low lattice energy would be more appropriate for PEO-based SPEs, whose chemical structures are shown in Figure 1c. The key difference between these two salts is derived from the chemical bonding of F. The S−F bond of NaFSI is unstable and easily broken at very low energies, whereas the C−F bond of NaTFSI is chemically very stable in most solvents. Therefore, NaFSI was chosen as the salt to take advantage of its controlling reaction with the solvent.[30,31]

As for the solvent, two requirements need to be satisfied. First, it should be able to dissolve PEO to form a uniform slurry. Second, its reaction with FSI^- must be controlled and be temperature- and time-dependent. Among the common solvents that can dissolve PEO, H_2O can hydrolyze the FSI^- at the controlling reaction rate, which is demonstrated by a simple aqueous solution static experiment. The pHs of the 0.5 M NaFSI aqueous solution and 0.5 M NaTFSI aqueous solution, with resting times, are shown in Figure S1. At the beginning, both of the fresh solutions are neutral. Remaining at room temperature (RT), the pH values of both solutions do not change much, meaning that the FSI^- hydrolysate reaction is very slow, or even negligible, at RT. Thereafter, we designed an accelerated reaction experiment: the solutions were put into an oven at a temperature of 80 °C and the pH values were recorded every day. The pH value of the NaFSI aqueous solution decreased markedly with the resting time. It was observed that the FSI^- hydrolyzed with H_2O to release hydrofluoric acid but that the reaction rate is controllable by temperature and time. Thus, distilled water was selected as the solvent, which is the cheapest and most environmentally

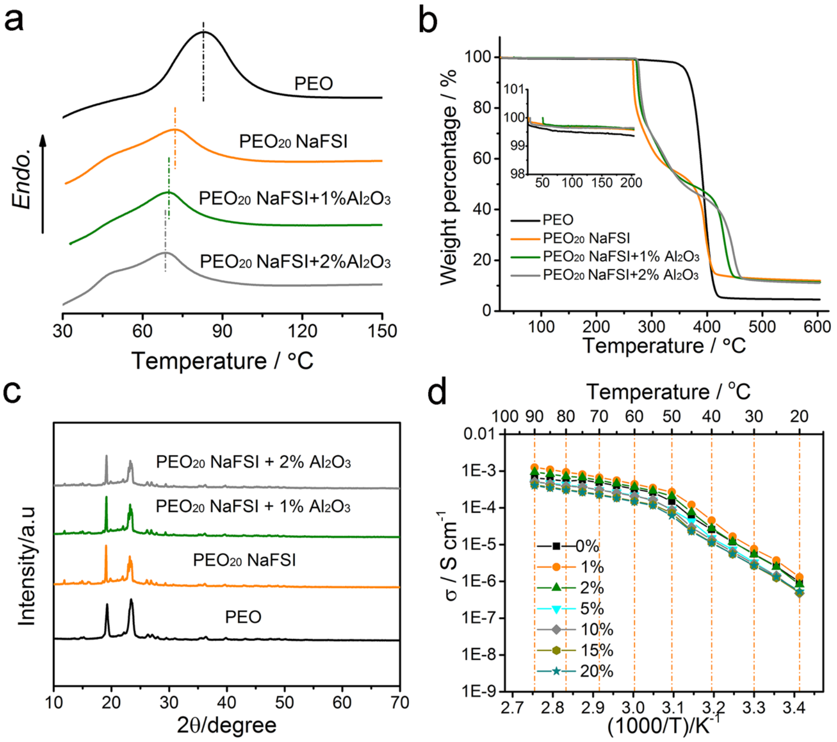

Figure 2. Characterization of the neat PEO and as-prepared $PEO_{20}NaFSI$ + x wt % Al_2O_3 (x = 0, 1, 2) blended polymer electrolyte: (a) DSC traces from 30 to 150 °C; (b) TGA traces from 30 to 600 °C (the inset is an enlarged image from 30 to 200 °C); (c) XRD; (d) temperature dependence of ionic conductivities for $PEO_{20}NaFSI$ + x wt % Al_2O_3 (x = 0, 1, 2, 5, 10, 15, 20) blended polymer electrolyte.

friendly among all of the solvents. Subsequently, in order to absorb the hydrolyzed product of HF, Al_2O_3 nanoparticles were added into the SPE. The pH value increased after Al_2O_3 nanoparticles were added into the above acid NaFSI solution (Figure S1), meaning that the HF was gradually neutralized. On one hand, Al_2O_3 will react with HF spontaneously to form $AlF_3{\cdot}xH_2O$; on the other hand, Al_2O_3 nanoparticles can increase the amorphous area of the PEO, thus leading to a higher ionic conductivity. The final design of the PEO-based SPE is aqueous PEO/NaFSI-Al_2O_3 with a reaction process as follows:

$$\text{NaFSI} + H_2O \rightarrow \text{HF} + \text{R-}SO_3H \tag{1}$$

$$\text{HF} + Al_2O_3 + H_2O \rightarrow AlF_3{\cdot}xH_2O \tag{2}$$

The as-prepared FSI-1%Al_2O_3-AQ blended polymer electrolyte is shown in Figure S2a, which is a semitransparent flexible membrane. The SEM image of the membrane section shows that the thickness is around 200 μm (Figure S2b). It is also clear from SEM images that the as-prepared membrane is relatively homogeneous and compact (inset in Figure S2b). Energy-dispersive X-ray (EDX) mapping analysis was performed to investigate the distribution of the components in the membrane. As shown in Figure S2c, the typical elements C, F, and Al, which represent PEO, NaFSI, and Al_2O_3, respectively, distribute uniformly. Figure 2a displays the differential scanning calorimetry (DSC) traces of the $PEO_{20}NaFSI$ + x wt % Al_2O_3 (x = 0, 1, 2; FSI- x%Al_2O_3-AQ) blended polymer electrolytes, as well as the pure PEO membrane. An endothermic peak at about 60—70 °C is observed in these SPEs, which corresponds to the melting temperature (T_m) of crystalline PEO. The T_m and melting enthalpy decrease with the increase of 1%Al_2O_3 nanoparticles, indicating an increased amount of amorphous phase formation, which benefits ion transport. This would be attributed to the plasticizing effects of nanoparticles on PEO, as reported by Croce et al. in 1998.[33] Furthermore, by calculating the integral area of the melting peak, the crystallinity of the samples is obtained, as shown in Table S1. The crystallinities of PEO, FSI-AQ, FSI-1%Al_2O_3, and FSI-2%Al_2O_3 are calculated to be 63.8, 30.7, 29.2, and 31.4%. Compared with pure PEO (reported as 196 J g^{-1}),[32] the crystallinity is greatly reduced when NaFSI is introduced, and the FSI-1%Al_2O_3 sample has the lowest crystallinity, which is consistent with the conductivity results as well. The thermal stabilities of the electrolytes as well as the PEO were determined by TGA tests. As shown in Figure 2b, the decomposition temperatures of these electrolytes are all higher than 265 °C, which are stable enough for use as a SPE for application in solid-state sodium batteries. X-ray diffraction (XRD) patterns of the FSI-x%Al_2O_3-AQ (x = 0, 1, 2) blended polymer electrolytes are presented in Figure 2c. Two characteristic diffraction peaks of the crystalline PEO, at 2θ = 19.2 and 23.3°, are observed.[28] Compared with neat PEO, the main peak at 2θ = 23.3° of the FSI-x%Al_2O_3-AQ (x = 0, 1, 2) SPEs became relatively weak. With the addition of the Al_2O_3 nanoparticles, the peaks appear to be slightly broader, confirming the decreased crystallinity of the PEO. This phenomenon in the XRD patterns is in good agreement with the DSC results. The ionic conductivities of the membranes (Al_2O_3 addition varying from 0 to 20 wt %) are shown in Figure 2d. Among them, the FSI-1%Al_2O_3-AQ exhibits the best ionic conductivity: 9.52×10^{-4} S cm^{-1} at 80 °C.

In order to further verify the uniqueness of our SPE ($PEO_{20}NaFSI$ + 1 wt % Al_2O_3-AQ (FSI-1%Al_2O_3-AQ)), two control SPEs with single variation were prepared, $PEO_{20}NaFSI$

DOI: 10.1021/acsenergylett.9b00857
ACS Energy Lett. 2019, 4, 1650−1657

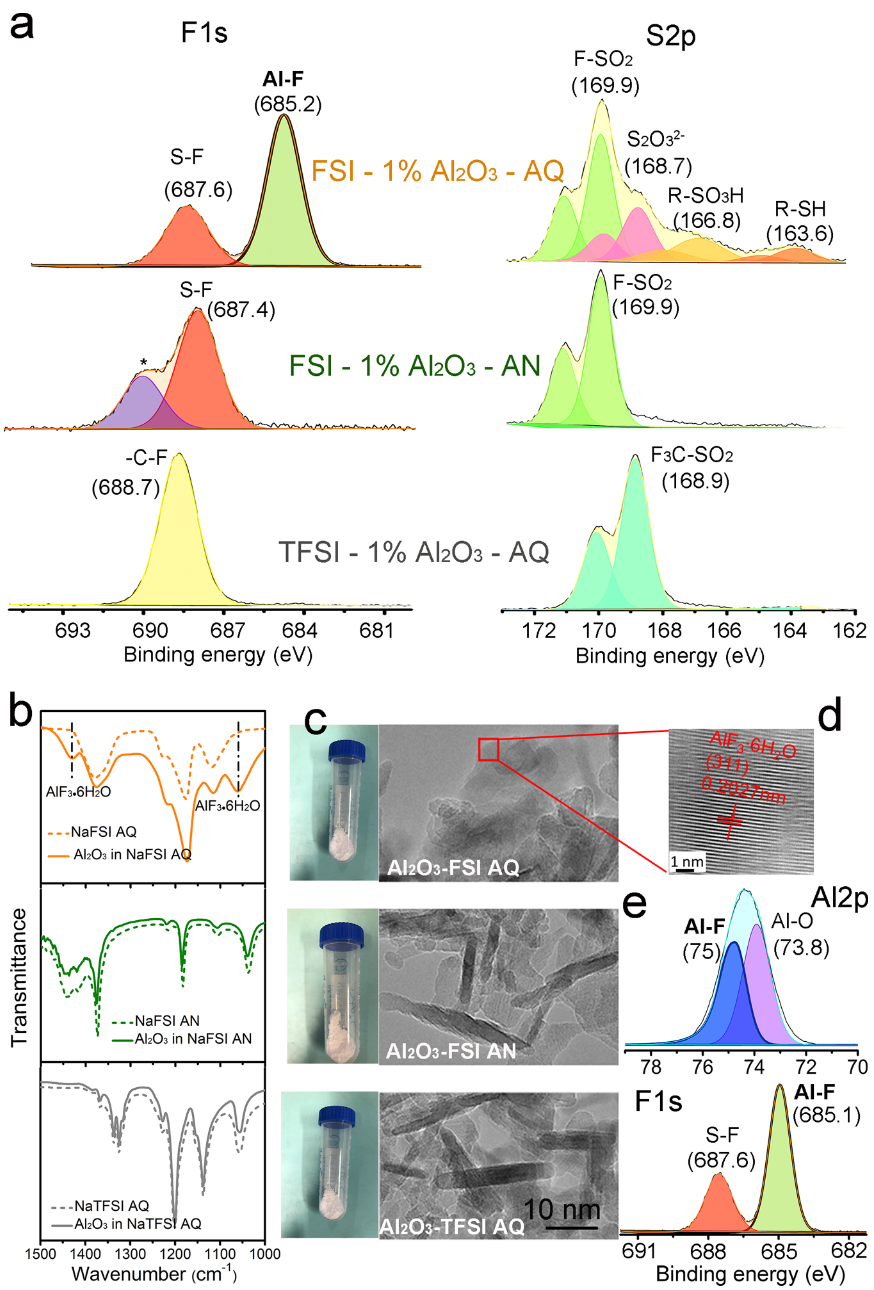

Figure 3. Characterizations of the SPEs, Na salt solutions, and Al_2O_3 powder filtrated from different Na salt solutions. (a) XPS spectra of F1s and S2p of the SPEs $PEO_{20}NaFSI$-1%Al_2O_3-AQ (aqueous), $PEO_{20}NaFSI$-1%Al_2O_3-AN (acetonitrile), and $PEO_{20}NaTFSI$-1%Al_2O_3-AQ. (b) Comparative FTIR spectra of Na salt solutions and solutions with Al_2O_3 powder added after stirring at 55 °C for 12 h. (c) Optical photographs and TEM images of the Al_2O_3 particles filtrated out from NaFSI aqueous solution (Al_2O_3-FSI-AQ), NaFSI acetonitrile solution (Al_2O_3-FSI-AN), and NaTFSI aqueous solution (Al_2O_3-TFSI-AQ) after stirring at 55 °C for 12 h followed by washing six times. (d) High-resolution TEM image of Al_2O_3-FSI-AQ. (e) XPS spectra of Al2p and F1s of the Al_2O_3-FSI-AQ.

+ 1 wt % Al_2O_3 with acetonitrile as the solvent (FSI-1%Al_2O_3-AN), and $PEO_{20}NaTFSI$ + 1 wt % Al_2O_3 with distilled water as the solvent (TFSI-1%Al_2O_3-AQ).

The XPS spectra shown in Figure 3a are the F1s and S2p spectra of FSI-1%Al_2O_3-AQ, FSI-1% Al_2O_3-AN, and TFSI-1% Al_2O_3-AQ SPEs. The fitted XPS spectra of F1s indicate that the elemental F in the designed FSI-1%Al_2O_3-AQ membrane is composed of S−F (NaFSI, 687.6 eV) and Al−F (685.2 eV), demonstrating the hydrolysis of NaFSI and production of HF. HF reacts with Al_2O_3 to form an aluminum fluoride compound. The S2p spectra of the FSI-1% Al_2O_3-AQ show that there are other spectral peaks (e.g., $S_2O_3^{2-}$ (168.7 eV), R−SO_3H (166.8 eV), and R−SH (163.6 eV)) besides NaFSI (F−SO_2, 169.9 eV), further providing evidence of the interaction between the salt NaFSI and water. For the other two membranes, however, no Al−F peak was observed in the fitted F 1s spectra, and there was only one pair of peaks ($S2p^1$ and $S2p^3$) attributed to the salt NaFSI or NaTFSI in the fitted S2p spectra.

FTIR measurements on different kinds of solution and the corresponding Al_2O_3 suspension were carried out to further demonstrate the special reaction in the designed electrolyte, as presented in Figures 3b and S3. In the spectra of Al_2O_3 in NaFSI aqueous solution, there are two characteristic peaks of

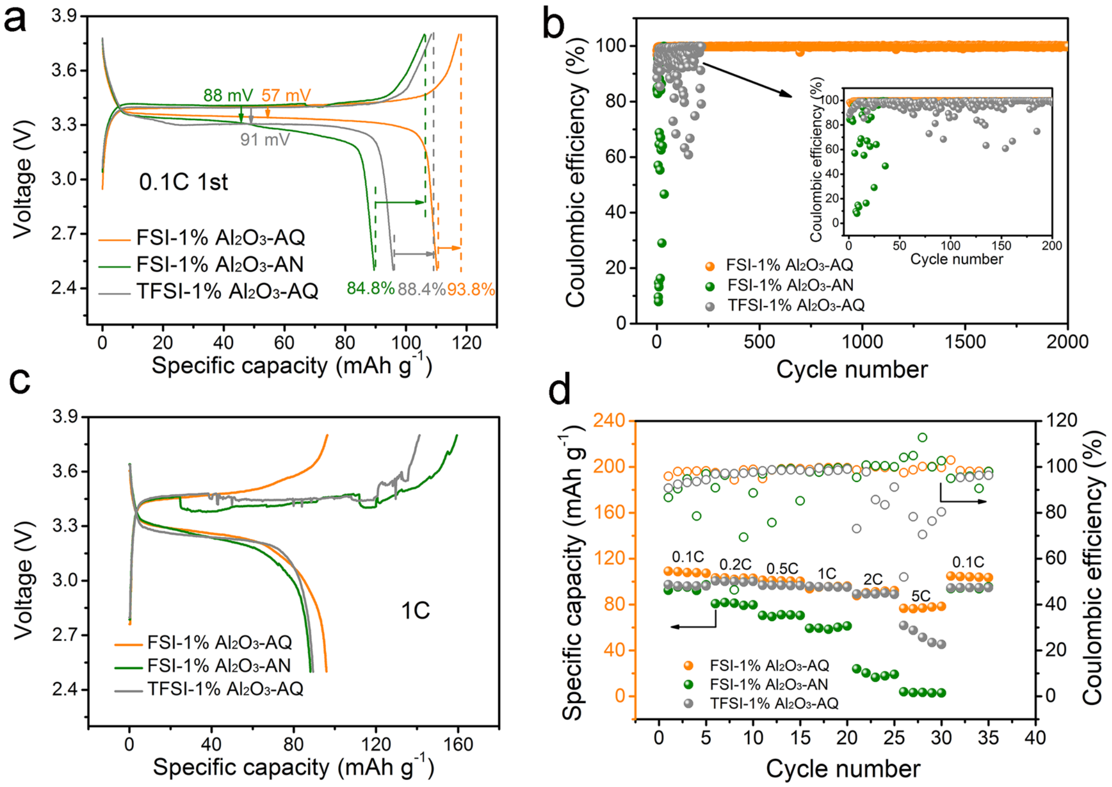

Figure 4. Electrochemical performance of the cells NVP|SPEs|Na with FSI-1%Al_2O_3-AQ, FSI-1%Al_2O_3-AN, or TFSI-1%Al_2O_3-AQ as he electrolyte at 80 °C. (a) First charge and discharge curves at the 0.1C rate. (b) Coulombic efficiencies at the 1C rate. (c) Typical charge and discharge curves at the 1C rate. (d) Rate performance from 0.1C to 5C.

$AlF_3 \cdot 6H_2O$, near the positions of 1430 and 1058 cm^{-1}, which can be assigned to the deformation mode of crystal water $\delta(H_2O)$ in $AlF_3 \cdot 6H_2O$ and the deformation vibration of −OH groups, respectively.[34] However, in another two FTIR spectra of Al_2O_3 in NaTFSI-AQ and NaFSI-AN, the peaks are not changed before and after adding Al_2O_3. Subsequently, the Al_2O_3 suspensions from different solutions were centrifuged and washed with the corresponding solvent six times to filtrate out the soluble salt, followed by drying. TEM graphs of the obtained powders (Figures 3c and S4) provide visual evidence that Al_2O_3 powder indeed reacts with NaFSI aqueous solution according to the obvious morphological changes of Al_2O_3 in FSI-AQ, which totally transforms from a pristine nanorod of length > 20 nm (Al_2O_3−P, Figure S4a) into a nanoparticle of less than 10 nm. The interplanar space of the particle out-layer is about 0.2027 nm, identical to the perfect crystalline $AlF_3 \cdot 6H_2O$ (0.2026 nm (311)) (Figure 3d). The XPS spectra of Al_2O_3-FSI-AQ are shown in Figures 3e and S5, and the fitted Al2p spectrum shows two peaks related to Al−O (73.8 eV) and Al−F (75 eV). The fitted F1s spectrum shows S−F (687.6 eV) and F−Al (685.1 eV). It should be noted that the quantities of the elements S and N are very small, and the element Na is water-soluble and filtered out. The atomic ratio of F, S, and N is about 89.79:6.26:3.95 (Figure S5), which is far from the original ratio of 2:2:1, verifying again that the F had been reacted with the Al_2O_3 and the product is water-insoluble.

Based on the results of XPS, FTIR, and TEM discussed above, it is concluded that the hydrolysate reaction indeed occurs in NaFSI aqueous solution. Furthermore, it is concluded that the presence of Al_2O_3 nanoparticles is confirmed, and the insoluble aluminum fluoride compound forms on the surface of the Al_2O_3 particles. This reaction spontaneously fixes the residual free water into hydration compounds in the membrane, which is chemically and electrochemically inert during the charging. It has also been reported in aqueous lithium/sodium ion batteries that the electrolyte becomes more stable when free water is bonded.[35,36] Moreover, the formed aluminum fluoride compound is more stable (AlF_3 reacts neither with acids nor with bases) and suppresses side reactions, thus improving the interfacial stability.

To evaluate the electrochemical performance of our SPE (FSI-1%Al_2O_3-AQ), the SSB is assembled with a carbon-coated $Na_3V_2(PO_4)_3$ (abbreviated as NVP) cathode and a Na metal anode. The fabricated NVP|FSI-1%Al_2O_3-AQ|Na coin-type cells were charged and discharged at the 0.1C rate, between 2.5 and 3.8 V, at 80 °C. As shown in Figure 4a, during the first cycle, the battery employing our SPE delivers a highly reversible specific capacity of 110 mAh g^{-1} with a high Coulombic efficiency of 93.8% and a very small polarization of 57 mV, whose capacity is an equivalent of 93.2% of the NVP's theoretical capacity (118 mAh g^{-1}), calculated from a single-electron process of the V^{4+}/V^{3+} redox couple. The batteries with the other control SPEs (FSI-1%Al_2O_3-AN and TFSI-1% Al_2O_3-AQ) have much lower reversible capacities (89 and 97 mAh g^{-1}, respectively) and initial Coulombic efficiencies (84.8 and 88.4%, respectively). Moreover, the polarizations are also larger (88 mV for FSI-1%Al_2O_3-AN and 91 mV for TFSI-1% Al_2O_3-AQ) than our designed FSI-1%Al_2O_3-AQ electrolyte. Figure 4b displays the Coulombic efficiencies of the batteries NVP|SPE|Na with the three different SPEs FSI-1%Al_2O_3-AQ, FSI-1%Al_2O_3-AN, and TFSI-1%Al_2O_3-AQ. The battery with our designed SPE FSI-1%Al_2O_3-AQ exhibits a high and steady

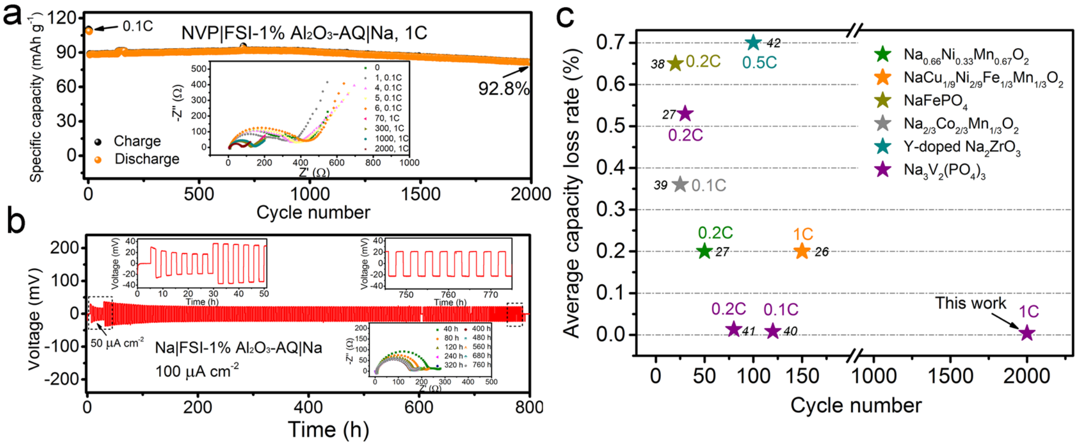

Figure 5. Cycling performance at 80 °C and performance summary of solid-state sodium batteries based on various SPEs and cathodes. (a) Long-term cycling performance of the cell NVP|FSI-1%Al_2O_3-AQ|Na at the 1C rate and the EIS (inset) during the working process. (b) Cycling performance for the symmetric cell Na|FSI-1%Al_2O_3-AQ|Na at a current density of 0.1 mA cm^{-2} and insets showing the magnified curve from 0 to 50 h and 745 to 775 h, as well as the EIS during the working process. (c) Average capacity loss rate and corresponding cycle number of solid-state sodium batteries based on various SPEs and cathodes.

Coulombic efficiency (∼100%) until the 2000th cycle, which is far superior to that of the control samples, wherein random fluctuations of Coulombic efficiencies are observed. The typical charge and discharge curves at the 1C rate are shown in Figure 4c. The charge curves of the cells employing the two control SPEs display obvious electrochemical decomposition behavior, indicating that the interface between the electrode and electrolyte is unstable. The rate performance is shown in Figure 4d. The cell NVP|FSI-1%Al_2O_3-AQ|Na exhibits better rate capability with reversible capacities of 110, 103.7, 100.6, 95.2, 91.5, and 76.8 mAh g^{-1} at rates of 0.1C, 0.2C, 0.5C, 1C, 2C, and 5C, respectively, while the cells with the other two control SPEs show poorer rate performance. Regarding Coulombic efficiency, random fluctuations of Coulombic efficiencies are observed in NVP|FSI-1%Al_2O_3-AN|Na and NVP|TFSI-1%Al_2O_3-AQ|Na cells. All of these comparison results illustrate that our strategy for designing a SPE is effective.

The superior long-term cycling stability is evaluated by the constant current charge−discharge test at rates of 1C (Figure 5a) and 2C (Figure S6), whose capacity retentions are 92.8 and 94.0% after 2000 cycles, respectively, with Coulombic efficiencies of nearly 100%. The electrochemical impedance spectra (EIS) at different cycle numbers are shown in the inset of Figure 5a. Before cycling, the EIS of the cell NVP|FSI-1% Al_2O_3-AQ|Na is about 450 Ω, which is much lower than that of the NVP|FSI-1%Al_2O_3-AN|Na (2750 Ω) and NVP|TFSI-1% Al_2O_3-AQ|Na (3500 Ω) (Figure S7a), indicating that the interface formed before cycling between the FSI-1%Al_2O_3-AQ electrolyte and electrodes is much more stable and highly ionic conducting. As shown in Figure 5a, the impedance of the cell NVP|FSI-1%Al_2O_3-AQ|Na remains at ∼400 Ω at the 0.1C rate and then decreases to ∼150 Ω when the current rate is changed to 1C. The impedance is relatively stable at both small and large current rates, proving the stability of the interfaces formed. While the EIS of the batteries employing the other two control SPEs show unstable values (Figure S7b,c), the comparative EIS behaviors both before cycling and during the charge−discharge process demonstrate that the designed FSI-1%Al_2O_3-AQ has an obvious superiority in stabilizing the interface. In addition, the Na|FSI-1%Al_2O_3-AQ|Na symmetrical battery was tested at a current density of 0.1 mA cm^{-2} to evaluate the interfacial compatibility of the electrolyte with Na metal. The polarization potential decreased gradually in the first few cycles and is then maintained at the low value of 21 mV for 800 h (200 cycles, Figure 5b). Electrochemical impedance spectroscopy was carried out simultaneously during the cycling (the inset in Figure 5b). The total impedance decreased in the initial few cycles and then stabilized at ∼170 Ω in the subsequent cycle time. Compared with all of the previous solid-state sodium polymer batteries,[26,27,37−42] the SSB with our SPE shows the lowest average capacity loss rate of 0.0036% and the longest cycle life of over 2000 cycles (Figure 5c, Table S2).

The aforementioned results indicate that relatively stable interfaces are formed between the designed FSI-1%Al_2O_3-AQ electrolyte and electrodes (NVP cathode and Na metal), which are superior to the two control samples (FSI-1%Al_2O_3-AN and TFSI-1%Al_2O_3-AQ), wherein the random fluctuations of Coulombic efficiencies (Figure 4b) and EIS (Figure S7) of the NVP|SPEs|Na SSBs were observed. Similar electrochemical behavior was observed in the FSI-AQ (without oxide additives) electrolyte (Figure S8) during the cycling process. The additive Al_2O_3 can help consume the hydrolysate HF, thereby contributing to the removal of H_2O. Without Al_2O_3, the residual HF and H_2O will cause interfacial side reactions. Furthermore, we prepared another electrolyte FSI-1%SiO_2-AQ by replacing Al_2O_3 with SiO_2 and tested the electrochemical performance. The charge and discharge curves, rate performance, and long-term cycling performance of the cell NVP|FSI-1%SiO_2-AQ|Na are shown in Figure S9, which are as good as those of NVP|FSI-1%Al_2O_3-AQ|Na. The FTIR spectra of FSI-1%SiO_2-AQ, FSI-1%SiO_2-AN, and TFSI-1%SiO_2-AQ membranes were also compared, and the results are shown in Figure S10. Consistent with the Al_2O_3 system, there is a Si−F stretching vibration peak (∼881 cm^{-1}) in the FSI-1%SiO_2-AQ membrane[43] but not in the other two. All of these results confirm the feasibility of our design for a SPE with stable interfacial compatibility. Furthermore, the FSI-Al_2O_3/SiO_2-AQ SPEs using water instead of acetonitrile as the solvent realize environmentally friendly and low-cost preparation of PEO-based SPEs.

DOI: 10.1021/acsenergylett.9b00857
ACS Energy Lett. 2019, 4, 1650−1657

In summary, we propose a new strategy to prepare high-quality SPEs for advanced rechargeable SSBs. Our principle is to design a spontaneous two-step chemical reaction to transfer the residual free solvent into an electrochemically inert compound so as to avoid electrochemical side reactions and stabilize the interface. We choose NaFSI and H_2O as the demonstrated salt and solvent, respectively, because the FSI^- can be hydrolyzed to consume residual water, and the hydrolysis is controllable by temperature change. Al_2O_3 nanoparticles as the proton acceptor are introduced to chemically absorb the hydrolysis product HF and form an electrochemical intermediate compound $AlF_3·6H_2O$. Furthermore, it is more environmentally friendly and cost-effective using water instead of traditional acetonitrile as the solvent to prepare SPEs. The SSB NVP|FSI-1%Al_2O_3-AQ|Na exhibits a reversible capacity of 110 mAh g^{-1} with a high initial Coulombic efficiency of 93.8% and good long-term cycling performance, with capacity retention of 92.8%/94% after 2000 cycles at 1C/2C rates, meaning that the average capacity loss rate is only 0.0036%/0.003%, respectively. The Na|FSI-1% Al_2O_3-AQ|Na symmetrical cell also delivers long-term cycling stability for up to 800 h. All of the results prove that our strategy to design SPEs able to self-regulate their solvent is effective. This work reveals the nature of the reaction process of the common PEO-NaFSI/NaTFSI-based SPEs from a novel perspective, which can also be extended to lithium-based SPEs (using LiFSI as the salt instead of LiTFSI), and could undoubtedly play a guiding role in designing high-performance SPEs.

■ ASSOCIATED CONTENT

Ⓢ Supporting Information

The Supporting Information is available free of charge on the ACS Publications website at DOI: 10.1021/acsenergylett.9b00857.

> Detailed description of experiment, including fabrication and characterization of SPEs, preparation of cathode materials and electrode sheets, cell fabrication and performance evaluation; supporting figures, including pH values, photograph and SEM images of SPEs, FTIR spectra, TEM images, XPS spectra, electrochemical performances and electrochemical impedance spectra; and supporting tables showing the crystallinity of SPEs and the comparison of electrochemical performances of PEO-based electrolytes for sodium batteries (PDF)

■ AUTHOR INFORMATION

Corresponding Authors

*E-mail: yshu@iphy.ac.cn (lead contact).
*E-mail: suoliumin@iphy.ac.cn.

ORCID

Lilu Liu: 0000-0002-2992-7577
Hong Li: 0000-0002-8659-086X
Yong-Sheng Hu: 0000-0002-8430-6474

Author Contributions

#L.L. and X.Q. contributed equally.

Notes

The authors declare no competing financial interest.

■ ACKNOWLEDGMENTS

This work was supported by the National Key Technologies R&D Program, China (2016YFB0901500) and the National Natural Science Foundation of China (51725206, 51421002 and 51822211)

■ REFERENCES

(1) Pan, H.; Hu, Y.-S.; Chen, L. Room-temperature stationary sodium-ion batteries for large-scale electric energy storage. *Energy Environ. Sci.* **2013**, *6*, 2338−2360.

(2) Kim, S.-W.; Seo, D.-H.; Ma, X.; Ceder, G.; Kang, K. Electrode materials for rechargeable sodium-ion batteries: Potential Alternatives to Current Lithium-Ion Batteries. *Adv. Energy Mater.* **2012**, *2*, 710−721.

(3) Palomares, V.; Serras, P.; Villaluenga, I.; Hueso, K. B.; Carretero-Gonzalez, J.; Rojo, T. Na-ion batteries, recent advances and present challenges to become low cost energy storage systems. *Energy Environ. Sci.* **2012**, *5*, 5884−5901.

(4) Zhao, C.; Liu, L.; Qi, X.; Lu, Y.; Wu, F.; Zhao, J.; Yu, Y.; Hu, Y.-S.; Chen, L. Solid-State Sodium Batteries. *Adv. Energy Mater.* **2018**, *8*, 1703012.

(5) Kim, J.-J.; Yoon, K.; Park, I.; Kang, K. Progress in the development of sodium-ion solid electrolytes. *Small Methods* **2017**, *1*, 1700219.

(6) Hu, Y.-S. Batteries: Getting solid. *Nat. Energy* **2016**, *1*, 16042.

(7) Liu, L.; Qi, X.; Shao, Y.; Pan, D.; Bai, Y.; Hu, Y.-S.; Chen, L. Reserch progress on sodium ion solid-state elctrolytes. *Energy Storage Science and Technology* **2017**, *6*, 961−980.

(8) Liu, L.; Qi, X.; Ma, Q.; Rong, X.; Hu, Y.-S.; Zhou, Z.; Li, H.; Huang, X.; Chen, L. Toothpaste-like electrode: A novel approach to optimize the interface for solid-state sodium-ion batteries with ultralong cycle life. *ACS Appl. Mater. Interfaces* **2016**, *8*, 32631−32636.

(9) Manthiram, A.; Yu, X.; Wang, S. Lithium battery chemistries enabled by solid-state electrolytes. *Nat. Rev. Mater.* **2017**, *2*, 16103.

(10) Ray, A. K.; Subbarao, E. C. Synthesis of sodium β- and β''-alumina. *Mater. Res. Bull.* **1975**, *10*, 583−590.

(11) Goodenough, J. B.; Hong, H. Y. P.; Kafalas, J. A. Fast Na^+-ion transport in skeleton structures. *Mater. Res. Bull.* **1976**, *11*, 203−220.

(12) Ribes, M.; Barrau, B.; Souquet, J. L. Sulfide glasses: Glass forming region, structure and ionic conduction of glasses in Na_2S-XS_2 (X = Si; Ge), Na_2S-P_2S_5 and Li_2S-GeS_2 systems. *J. Non-Cryst. Solids* **1980**, *38*, 271−276.

(13) Moon, C. K.; Lee, H.-J.; Park, K. H.; Kwak, H.; Heo, J. W.; Choi, K.; Yang, H.; Kim, M.-S.; Hong, S.-T.; Lee, J. H.; Jung, Y. S. Vacancy-driven Na^+ superionic conduction in new Ca-doped Na_3PS_4 for all-solid-state Na-ion batteries. *ACS Energy Lett.* **2018**, *3*, 2504−2512.

(14) Fenton, D. E.; Parker, J. M.; Wright, P. V. Complexes of Alkali-Metal Ions with Poly(Ethylene Oxide). *Polymer* **1973**, *14*, 589−589.

(15) Zhang, Z.; Zhang, Q.; Shi, J.; Chu, Y. S.; Yu, X.; Xu, K.; Ge, M.; Yan, H.; Li, W.; Gu, L.; Li, H.; Yang, X.-Q.; Huang, X.; Chen, L.; et al. A self-forming composite electrolyte for solid-state sodium battery with ultra-long cycle life. *Adv. Energy Mater.* **2017**, *7*, 1601196.

(16) Shao, Y.; Wang, H.; Gong, Z.; Wang, D.; Zheng, B.; Zhu, J.; Lu, Y.; Hu, Y.-S.; Guo, X.; Li, H.; Huang, X.; Yang, Y.; Nan, C.-W.; Chen, L. Drawing a soft interface: An effective interfacial modification strategy for garnet type solid-state Li batteries. *ACS Energy Lett.* **2018**, *3*, 1212−1218.

(17) Zhou, C.; Bag, S.; Thangadurai, V. Engineering materials for progressive all-solid-state Na batteries. *ACS Energy Lett.* **2018**, *3*, 2181−2198.

(18) Tatsumisago, M.; Nagao, M.; Hayashi, A. Recent development of sulfide solid electrolytes and interfacial modification for all-solid-state rechargeable lithium batteries. *J. Asian Ceram. Soc.* **2013**, *1*, 17−25.

(19) Wan, H.; Mwizerwa, J. P.; Qi, X.; Liu, X.; Xu, X.; Li, H.; Hu, Y.-S.; Yao, X. Core−Shell $Fe_{1-x}S$@$Na_{2.9}PS_{3.95}Se_{0.05}$ nanorods for room

temperature all-solid-state sodium batteries with high energy density. *ACS Nano* **2018**, *12*, 2809−2817.

(20) Wan, H.; Mwizerwa, J. P.; Qi, X.; Xu, X.; Li, H.; Zhang, Q.; Cai, L.; Hu, Y. S.; Yao, X. Nanoscaled Na_3PS_4 solid electrolyte for all-solid-state FeS_2/Na batteries with ultrahigh initial coulombic efficiency of 95% and excellent cyclic performances. *ACS Appl. Mater. Interfaces* **2018**, *10*, 12300−12304.

(21) Takada, K.; Ohno, T.; Ohta, N.; Ohnishi, T.; Tanaka, Y. Positive and negative aspects of interfaces in solid-state batteries. *ACS Energy Lett.* **2018**, *3*, 98−103.

(22) Cheng, T.; Merinov, B. V.; Morozov, S.; Goddard, W. A. Quantum mechanics reactive dynamics study of solid Li-electrode/Li_6PS_5Cl-Electrolyte interface. *ACS Energy Lett.* **2017**, *2*, 1454−1459.

(23) Di Noto, V.; Lavina, S.; Giffin, G. A.; Negro, E.; Scrosati, B. Polymer electrolytes: Present, past and future. *Electrochim. Acta* **2011**, *57*, 4−13.

(24) Golodnitsky, D.; Strauss, E.; Peled, E.; Greenbaum, S. Review—on order and disorder in polymer electrolytes. *J. Electrochem. Soc.* **2015**, *162*, A2551−A2566.

(25) Berthier, C.; Gorecki, W.; Minier, M.; Armand, M. B.; Chabagno, J. M.; Rigaud, P. Microscopic investigation of ionic conductivity in alkali metal salts-poly(ethylene oxide) adducts. *Solid State Ionics* **1983**, *11*, 91−95.

(26) Ma, Q.; Liu, J.; Qi, X.; Rong, X.; Shao, Y.; Feng, W.; Nie, J.; Hu, Y.-S.; Li, H.; Huang, X.; Chen, L.; Zhou, Z. A new Na[(FSO_2)(n-$C_4F_9SO_2$)N]-based polymer electrolyte for solid-state sodium batteries. *J. Mater. Chem. A* **2017**, *5*, 7738−7743.

(27) Qi, X. G.; Ma, Q.; Liu, L. L.; Hu, Y. S.; Li, H.; Zhou, Z. B.; Huang, X. J.; Chen, L. Q. Sodium bis(fluorosulfonyl)imide/poly(ethylene oxide) polymer electrolytes for sodium-ion batteries. *ChemElectroChem* **2016**, *3*, 1741−1745.

(28) Ma, Q.; Qi, X.; Tong, B.; Zheng, Y.; Feng, W.; Nie, J.; Hu, Y.; Li, H.; Huang, X.; Chen, L.; Zhou, Z. B. Novel Li[(CF_3SO_2)(n-$C_4F_9SO_2$)N]-based polymer electrolytes for solid-state lithium batteries with superior electrochemical performance. *ACS Appl. Mater. Interfaces* **2016**, *8*, 29705−29712.

(29) Croce, F.; Curini, R.; Martinelli, A.; Persi, L.; Ronci, F.; Scrosati, B.; Caminiti, R. Physical and Chemical Properties of Nanocomposite Polymer Electrolytes. *J. Phys. Chem. B* **1999**, *103*, 10632−10638.

(30) Eshetu, G.; Diemant, T.; Grugeon, S.; Behm, R.; Laruelle, S.; Armand, M.; Passerini, S. In-Depth Interfacial Chemstry and Reactivity Focused Investigation of Lithium-Imide and Lithium-Imidazole-Based Electrolytes. *ACS Appl. Mater. Interfaces* **2016**, *8*, 16087−16100.

(31) Eshetu, G.; Judez, X.; Li, C.; Martinez-Ibanez, M.; Gracia, I.; Bondarchuk, O.; Carrasco, J.; Rodriguez-Martinez, L.; Zhang, H.; Armand, M. Ultrahigh Performance All Solid-State Lithium Sulfur Batteries: Salt Anion's Chemistry-Induced Anomalous Synergistic Effect. *J. Am. Chem. Soc.* **2018**, *140*, 9921−9933.

(32) Zardalidis, G.; Mars, J.; Allgaier, J.; Mezger, M.; Richter, D.; Floudas, G. Influence of Chain Topology on Polymer Crystallization: Poly(ethylene oxide)(PEO) Rings vs. Linear Chains. *Soft Matter* **2016**, *12*, 8124.

(33) Croce, F.; Appetecchi, G. B.; Persi, L.; Scrosati, B. Nanocomposite polymer electrolytesfor lithium batteries. *Nature* **1998**, *394*, 456−458.

(34) Wang, G.; Mudring, A.-V. The missing hydrate $AlF_3 \cdot 6H_2O$ $[Al(H_2O)_6]F_3$: Ionothermal synthesis, crystal structure and characterization of aluminum fluoride hexahydrate. *Solid State Sci.* **2016**, *61*, 58−62.

(35) Suo, L.; Borodin, O.; Gao, T.; Olguin, M.; Ho, J.; Fan, X.; Luo, C.; Wang, C.; Xu, K. Water-in-salt" electrolyte enables high-voltage aqueous lithium-ion chemistries. *Science* **2015**, *350*, 938−943.

(36) Suo, L.; Borodin, O.; Wang, Y.; Rong, X.; Sun, W.; Fan, X.; Xu, S.; Schroeder, M.; Cresce, A.; Wang, F.; Yang, C.; Hu, Y.; Xu, K.; Wang, C. Water-in-Salt" Electrolyte Makes Aqueous Sodium-ion Battery Safe, Green, and Long-Lasting. *Adv. Energy Mater.* **2017**, *7*, 1701189.

(37) Park, C.-W.; Ryu, H.-S.; Kim, K.-W.; Ahn, J.-H.; Lee, J.-Y.; Ahn, H.-J. Discharge properties of all-solid sodium−sulfur battery using poly (ethylene oxide) electrolyte. *J. Power Sources* **2007**, *165*, 450−454.

(38) Colò, F.; Bella, F.; Nair, J. R.; Destro, M.; Gerbaldi, C. Cellulose-based novel hybrid polymer electrolytes for green and efficient Na-ion batteries. *Electrochim. Acta* **2015**, *174*, 185−190.

(39) Ni'mah, Y. L.; Cheng, M.-Y.; Cheng, J. H.; Rick, J.; Hwang, B.-J. Solid-state polymer nanocomposite electrolyte of TiO_2/PEO/$NaClO_4$ for sodium ion batteries. *J. Power Sources* **2015**, *278*, 375−381.

(40) Zhang, Z.; Zhang, Q.; Ren, C.; Luo, F.; Ma, Q.; Hu, Y.-S.; Zhou, Z.; Li, H.; Huang, X.; Chen, L. A ceramic/polymer composite solid electrolyte for sodium batteries. *J. Mater. Chem. A* **2016**, *4*, 15823−15828.

(41) Zhang, Z.; Xu, K.; Rong, X.; Hu, Y.-S.; Li, H.; Huang, X.; Chen, L. $Na_{3.4}Zr_{1.8}Mg_{0.2}Si_2PO_{12}$ filled poly(ethylene oxide)/$Na(CF_3SO_2)_2N$ as flexible composite polymer electrolyte for solid-state sodium batteries. *J. Power Sources* **2017**, *372*, 270−275.

(42) Song, S.; Kotobuki, M.; Zheng, F.; Xu, C.; Savilov, S. V.; Hu, N.; Lu, L.; Wang, Y.; Li, W. D. Z. A hybrid polymer/oxide/ionic-liquid solid electrolyte for Na-metal batteries. *J. Mater. Chem. A* **2017**, *5*, 6424−6431.

(43) Simons, W W. *The Sadtler handbook of infrared spectra*; Sadtler Research Laboratories: Philadelphia, PA, 1978.